PERGAMON

International Journal of Solids and Structures 37 (2000) 4437–4453

INTERNATIONAL JOURNAL OF SOLIDS and STRUCTURES

www.elsevier.com/locate/ijsolstr

Identification of the through-thickness properties of thick laminated tubes using the virtual fields method

Fabrice Pierron[a], Sergei Zhavoronok[b], Michel Grédiac[c,*]

[a]*SMS/Département Mécanique et Matériaux, Ecole Nationale Supérieure des Mines de Saint-Etienne, 158, cours Fauriel, 42023, Saint-Etienne, Cedex 2, France*

[b]*Moscow State Aviation Institute, Technical University, Department 603, 125871, Volokolamskoie shosse 4, Moscow, Russia*

[c]*LERMES, Université Blaise Pascal, 24, avenue des Landais, 63174, Aubière, Cedex, France*

Received 14 November 1998; in revised form 25 March 1999

Abstract

This paper presents a method to determine the four through-thickness stiffnesses of thick laminated composites. Only one specimen submitted to one test is required. The procedure is based on a suitable use of the principle of virtual work with four independent virtual fields. This leads to a system of four linear equations where the through-thickness stiffnesses are the unknowns. The system is finally inverted to determine the stiffnesses. Finite element simulations have been carried out to validate the approach and to show its stability.

Keywords: Thick composites; Composite tubes; Through-thickness properties

1. Introduction

Structural composite components in the aerospace industry are usually composed of thin plates or shells for which the knowledge of the in-plane ply moduli and strengths are enough to design the structure. However, the extension of composite applications in other industrial sectors such as the naval or ground transportation fields requires the use of less costly materials such as glass reinforced polymers, for which increased thicknesses are usually necessary to fulfil the structural function. As a consequence, the plane stress and plane strain assumption of the classical lamination theory does not hold any more and full three-dimensional (3-D) stress and strain states must be taken into account for the design. It is, therefore, necessary for the designer to know not only the in-plane but also the through-thickness ply moduli and strengths.

* Corresponding author. Fax: +33-4-7340-7494.
E-mail address: grediac@lermes.univ-bpclermont.fr (M. Grédiac).

0020-7683/00/$ - see front matter
PII: S0020-7683(99)00149-3

Because of the relatively new development of such structures, the measurement of through-thickness properties has seldom been addressed by researchers on composites. A number of mechanical tests are however available, ranging from direct tensile test on a through-thickness waisted or non-waisted specimen (Broughton and Sims, 1994; Mespoulet, 1998) to through-thickness shear using the Iosipescu (Gipple and Hoyns, 1994) and/or the torsion test on rectangular rods and tension and/or bending on a curved specimen (Broughton and Sims, 1994; Hiel et al., 1991; ASTM, 1998). Nevertheless, these methods are not reliable mainly because of the difficulty to achieve homogeneous stress states in the specimens.

Alternative methods based on mixed experimental/numerical approaches have been proposed in the literature to measure elastic properties of composite plates (Sol, 1986; De Wilde, 1991; Hendriks, 1991; Pedersen and Frederiksen, 1992; Araujo et al., 1996; Frederiksen (1997, 1998); Rikards and Chate, 1998; Cunha and Piranda, 1999). The response of the tested specimen is modelled with a finite element programme or another approximation method like the Ritz method and the unknown parameters are adjusted stepwise, in such a way that both sets of measured and computed values of the displacements, strains or natural frequencies match as precisely as possible. These methods were first developed for measuring in-plane properties but some of them allow the determination of the through-thickness shear moduli (see Frederiksen, 1998 for instance) with a good accuracy. However, the transverse tensile moduli and Poisson's ratio are not determined with such methods. Moreover, a relevant initial guess for the values of the unknowns must be supplied to insure the convergence of the numerical procedure.

The aim of this paper is to describe an alternative method allowing the determination of the through-thickness stiffnesses from a testing configuration giving rise to heterogeneous stress fields inside the specimen. This method clearly departs from the above ones for the following reasons:

- four through-thickness elastic parameters are determined (not only the through-thickness shear modulus);
- no assumption is made concerning the through-thickness kinematic field, contrary to the dynamical methods where the displacement field is assumed to verify some theories like the higher-order shear deformation theory by Reddy (Frederiksen, 1998);
- the unknown parameters are determined directly, without any iterative calculations;
- a ring specimen is considered instead of a thick plate. The idea here is to measure elastic parameters of thick tubes that are very important for offshore applications (Pierron and Davies, 1998). Usual standard methods such as the Iosipescu test or the direct tension test cannot be used to characterize them. The ring is subjected to diametral compression. This testing configuration can be easily setup in practice using a universal tension/compression testing machine;
- the whole through-thickness kinematic field is assumed to be measured with a suitable optical technique. In the present work, however, the method itself is described and simulated with a finite element programme that provides the displacement and strain components at the nodes of the mesh. In practice, such kinematic fields would be obtained with a method derived from the grid method already used for characterizing in-plane properties of composite plates (Grédiac et al., 1999).

The theoretical aspects of the procedure are described in the first part of the paper. Some results of finite element simulations are then given for a specific specimen geometry. The stability of the procedure is finally examined.

2. Theory

2.1. Introduction

The method used here is based on a relevant use of the principle of virtual work. It was first

introduced by Grédiac (1989) for anisotropic plate bending problems, both in statics (Grédiac, 1996) and in dynamics (Grédiac et al., 1998a) and for in-plane problems (Grédiac and Pierron, 1998). The whole strain field is required for such a method. It can be obtained in practice with an optical method (Grédiac et al., 1999), but this point is not developed here. In the above references, only the in-plane or bending elastic properties of thin composite plates were measured. The objective here is different since the determination of through-thickness properties of thick composite tubes is addressed.

The basic idea is to apply the principle of virtual work to the tested specimen with some explicit and independent virtual displacement fields. Each new virtual field provides a new linear equation where the stiffnesses are unknown. This leads to a linear system which has to be inverted. This method is very general but two main difficulties arise in practice. First, one has to define a specimen geometry where the influences of each unknown are approximately balanced to ensure its 'identifiability'. Second, a set of admissible virtual fields leading to a well-conditioned system must be found. This will be solved in the following sections in the case of the determination of the through-thickness stiffnesses.

2.2. Principle of virtual work with specific virtual fields

An orthotropic medium characterised by four independent stiffnesses is considered. Because of the shape of the specimen studied below, polar coordinates are used. In this coordinate system and assuming a linear elastic behaviour, the independent stiffnesses to be identified relate the in-plane stress to the strain components as follows

$$\begin{pmatrix} \sigma_\theta \\ \sigma_r \\ \sigma_s \end{pmatrix} = \begin{pmatrix} Q_{\theta\theta} & Q_{\theta r} & 0 \\ Q_{\theta r} & Q_{rr} & 0 \\ 0 & 0 & Q_{ss} \end{pmatrix} \begin{pmatrix} \varepsilon_\theta \\ \varepsilon_r \\ \varepsilon_s \end{pmatrix} \tag{1}$$

where σ_i and ε_i, with $i, j = \theta, r, s$ are the components, of the stress and strain tensors, respectively (the classical contraction from 2 to 1 for the stress and strain indices is used), the Q_{ij}'s are the stiffnesses to be determined.

The present identification method is based on the principle of virtual work which can be written in the following form

$$-\int_V \sigma_{ij}\varepsilon^*_{ij}\,\mathrm{d}V + \int_{\partial V} T_i u^*_i\,\mathrm{d}S = 0 \tag{2}$$

where the convention of repeated indices for summation is adopted, V is the volume of the specimen considered, ∂V its boundary, σ the stress tensor, ε^* the virtual strain tensor, T the surface load density and u^* the virtual displacement field associated to ε^*. The first term is the internal virtual work and the second one is the external virtual work. Considering now that the problem is an in-plane one and that the specimen is subjected to a force applied at a point M, Eq. (2) becomes

$$\int_S \sigma_\theta\varepsilon^*_\theta\,\mathrm{d}S + \int_S \sigma_r\varepsilon^*_r\,\mathrm{d}S + \int_S \sigma_s\varepsilon^*_s\,\mathrm{d}S = \frac{Fu^*(M)}{e} \tag{3}$$

where e is the thickness of the specimen, S its surface, $u^*(M)$ the virtual displacement along the direction of the loading and F the magnitude of the load.

Introducing new Eq. (1) in Eq. (3) and assuming that the material properties are homogeneous over the specimen

$$Q_{\theta\theta}\int_S \varepsilon_\theta\varepsilon_\theta^* \,\mathrm{d}S + Q_{rr}\int_S \varepsilon_r\varepsilon_r^* \,\mathrm{d}S + Q_{\theta r}\int_S (\varepsilon_r\varepsilon_\theta^* + \varepsilon_\theta\varepsilon_r^*)\mathrm{d}S + Q_{ss}\int_S \varepsilon_s\varepsilon_s^* \,\mathrm{d}S = \frac{Fu^*(M)}{e} \tag{4}$$

As may be seen, a linear equation involving the four unknown stiffnesses is obtained. The objective is now to define the shape of the specimen and at least four independent virtual fields to build up a linear system where the stiffnesses are unknown.

2.3. Shape of the tested specimen

The choice of the specimen shape as well as of the loading conditions is somewhat arbitrary, but it must follow some obvious rules. For instance, the specimen must be easily manufactured and the magnitude of the three in-plane stress components inside the loaded specimen must be approximately balanced to ensure the 'identifiability' of the stiffnesses.

The geometry studied here is a thick ring obtained for instance from a thick composite tube (see Fig. 1). It is subjected to a unique radial force. The first point is to check that these loading conditions are relevant, i.e. that the magnitude of the three stress components are roughly the same. Hence, a finite element calculation has been carried out with the following material properties (glass fibre UD hoop wound ring):

$$E_{\theta\theta} = 40 \text{ GPa}, \quad E_{rr} = 10 \text{ GPa}$$

$$G_{\theta r} = 4 \text{ GPa}, \quad \nu_{\theta r} = 0.3 \tag{5}$$

These quantities are directly related to the unknown stiffnesses by the following formulae

$$E_{\theta\theta} = Q_{\theta\theta}\left(1 - \frac{Q_{\theta r}^2}{Q_{rr}Q_{\theta\theta}}\right), \quad E_{rr} = Q_{rr}\left(1 - \frac{Q_{\theta r}^2}{Q_{rr}Q_{\theta\theta}}\right), \quad \nu_{\theta r} = \frac{Q_{\theta r}}{Q_{rr}}, \quad G_{\theta r} = Q_{ss} \tag{6}$$

The model has been developed with the ANSYS 5.3 package. The following dimensions of this specimen have been used (see Fig. 2):

$$R_1 = 87.5 \text{ mm}, \quad R_0 = 37.5 \text{ mm}, \quad R = 62.5 \text{ mm}$$

$$h = 50 \text{ mm}, \quad e = 50 \text{ mm} \tag{7}$$

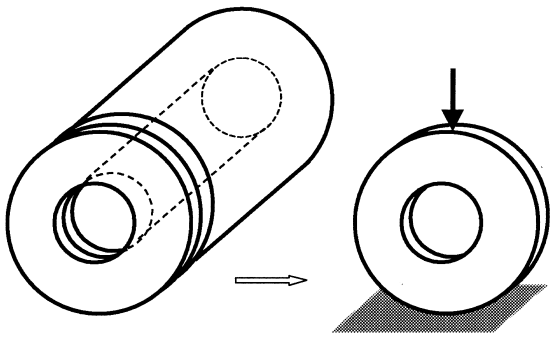

Fig. 1. Ring specimen cut in a thick composite tube.

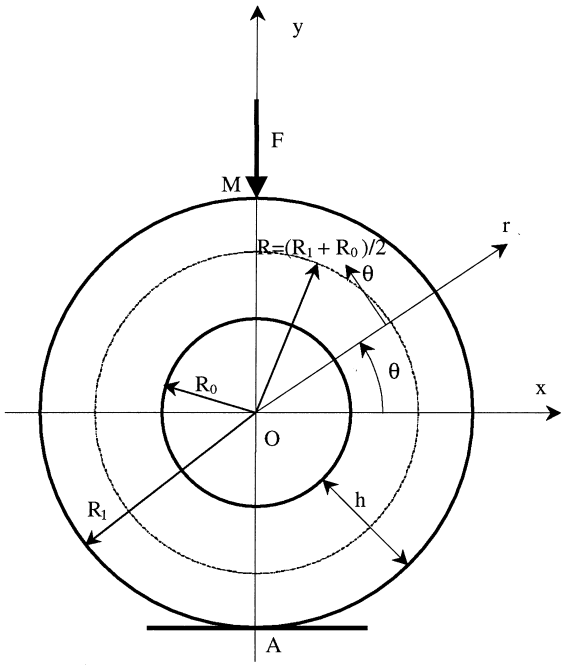

Fig. 2. Ring specimen.

Because of the symmetry of the problem, only one quarter of the ring has been considered and meshed with 1500 bilinear elements (plane 42): 30 along the width and 50 along the quarter of the circle. It has been checked with a convergence study that the results provided by the programme are satisfactory. The three in-plane stress contours are plotted in Figs. 3–5. As can be seen, the range of the three stress components are of roughly equal magnitudes, which confirms the potential 'identifiability' of the four stiffness components.

2.4. Virtual fields used for the identification procedure

2.4.1. Introduction

The problem is now to define four different virtual fields leading to four independent linear equations. Note that more than four fields could be used to obtain a redundant system, but this approach has not been retained in the present work. The virtual fields have only to be continuous and kinematically admissible. Hence, a wide range of choices is available for these fields, which will be defined following the general rules listed below:

1. the four fields must be independent to ensure the independence of the equations;
2. previous investigations carried out with a similar approach have shown that the literal expression of the fields must be as simple as possible to ensure the stability and the accuracy of the procedure;
3. to improve the independence of the equations, the fields must lead to partially uncoupled equations, i.e. only some of the unknowns must appear in the equations if possible. Ideally, the best choice should lead to an internal work in which only one stiffness is involved, but this is not always possible to achieve;

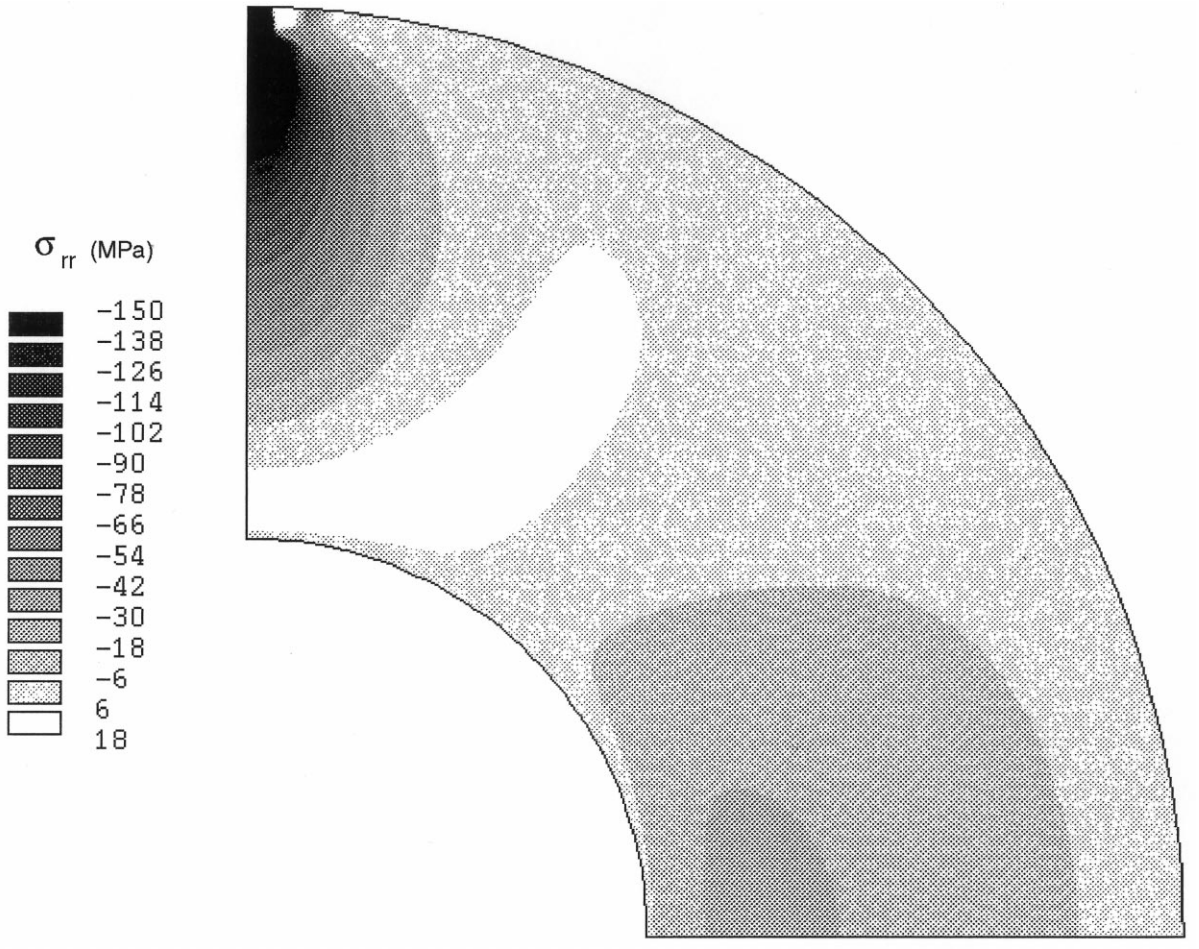

Fig. 3. Stress contour in the ring specimen: σ_r.

4. depending on the specimen geometry, either the whole surface of the specimen or only one particular part can be virtually deformed. In both cases however, the area where the virtual strain components are maximum must match as much as possible, the area where the actual stress components are maximum to reduce the influence of measurement errors on the actual strain on the internal virtual work.

There is no general rule providing automatically, the virtual fields for a given identification problem since this choice strongly depends on the shape of the specimen, on the loading and therefore, on the stress field itself inside the specimen which remains analytically unknown. As will be shown in the following section, the procedure for finding a set of initial fields leading to independent equations is mainly based on common sense and it is clear that this choice is not unique. This choice can be considered as satisfactory only a posteriori with numerical simulations. Note finally, that the virtual fields can be considered as filters which emphasize the contribution to the internal virtual work of some

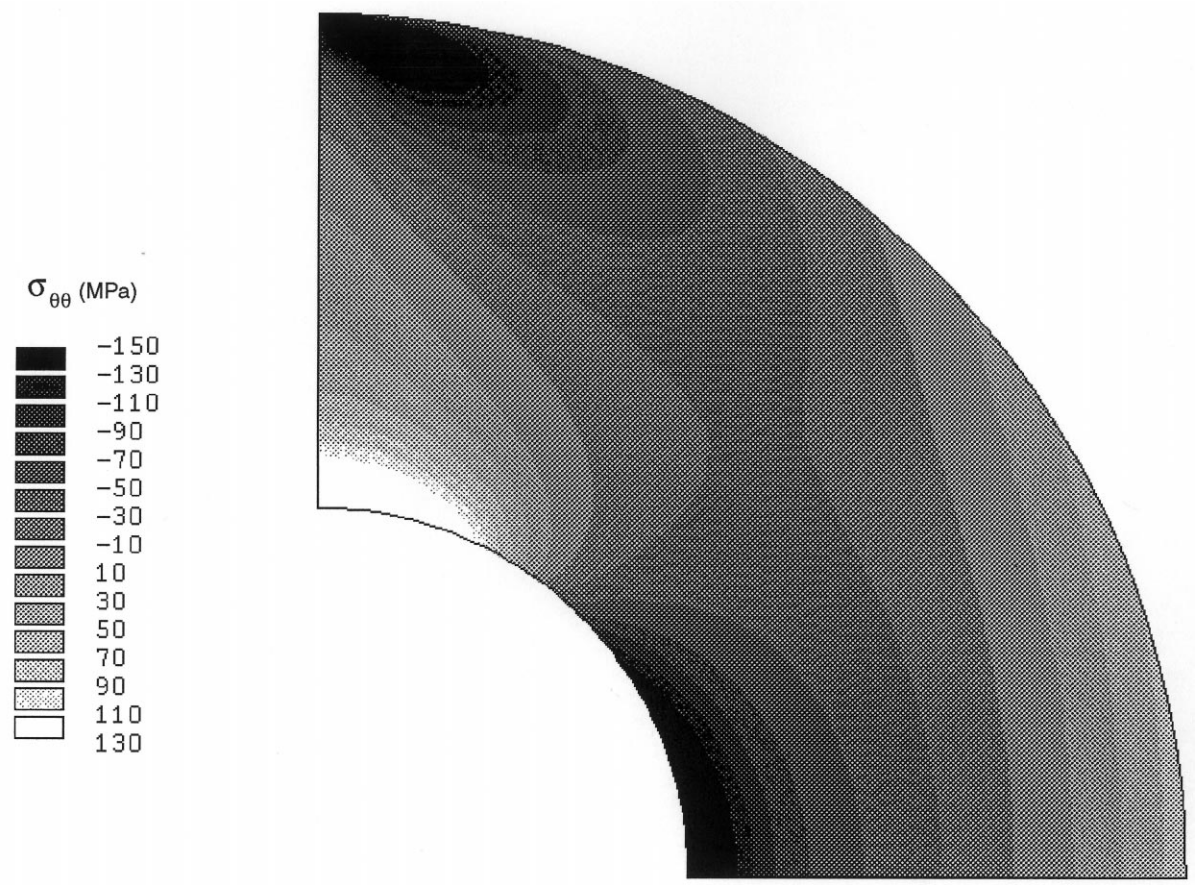

Fig. 4. Stress contour in the ring specimen: σ_θ.

unknowns or of some parts of the specimen. This feature is used to define the testing configurations and to choose the virtual fields in the present problem.

2.4.2. Virtual fields

The four fields defined for this specimen shape are shown in Figs. 6–9. The choice of these fields is more or less intuitive and somewhat arbitrary, but it is checked that they follow the above rules as much as possible and that they lead in practice to the unknown stiffnesses. Each of the following fields is of the form

$$\vec{u}^* = u_r^*\vec{e}_r + u_\theta^*\vec{e}_\theta + K\vec{e}_y \tag{8}$$

where u_r^*, u_θ^* are the virtual displacements in the natural polar coordinate system (O, r, θ) of the specimen (see Fig. 2), $\vec{e}_r$, $\vec{e}_\theta$ and $\vec{e}_y$ are normalized vectors along the r-, θ- and y-axes, respectively. $K\vec{e}_y$ is a constant global displacement that is adjusted in such a way that point A located at the bottom of the ring does not move. Hence, the virtual displacement field is admissible. Note that this constant term has no influence on the virtual strain field as it vanishes after differentiation.

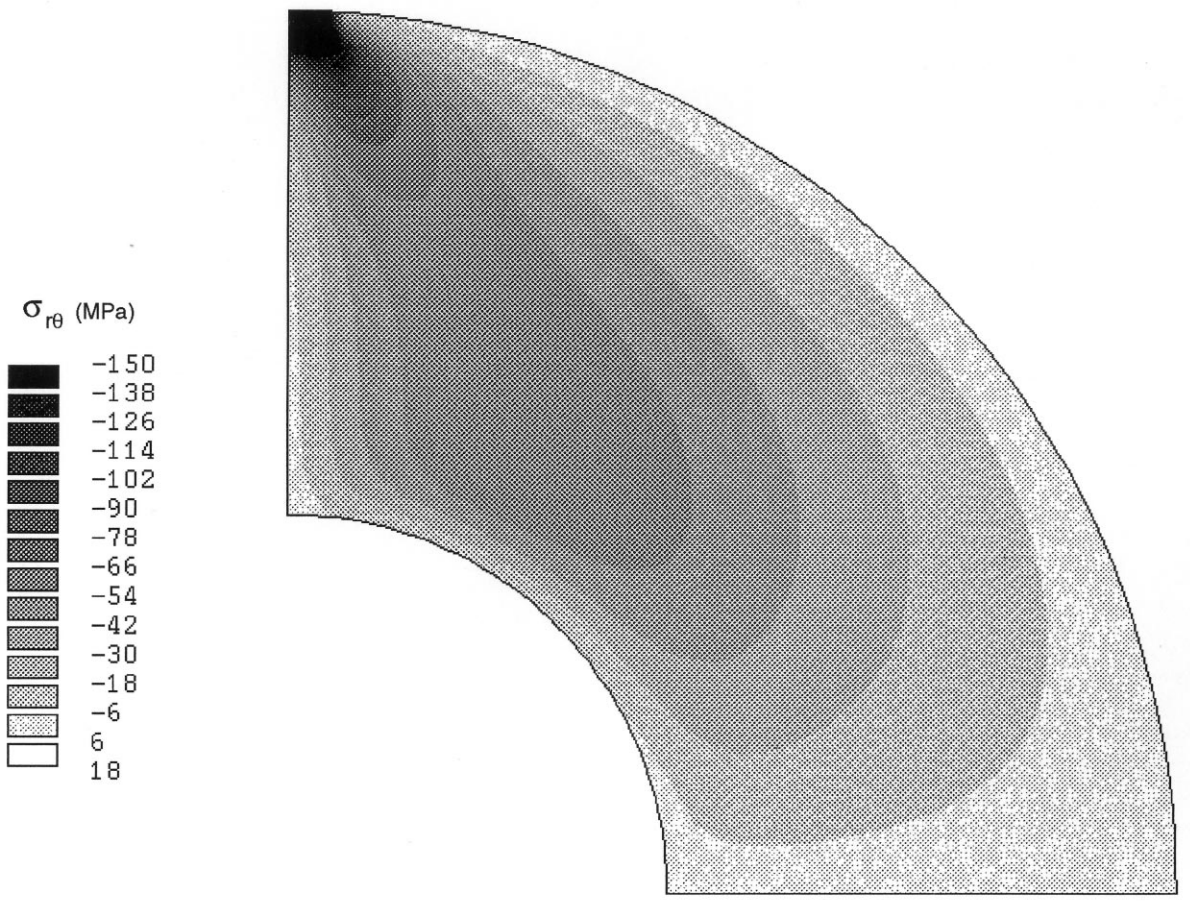

Fig. 5. Stress contour in the ring specimen: σ_s.

2.4.2.1. Field 1: virtual hydrostatical compression. The first field (see Fig. 6) can be considered as a virtual hydrostatical compression. It is defined by

$$u_r^* = -kr, \quad u_\theta^* = 0, \quad K = -kR_1 \tag{9}$$

where k is any non-zero real numbers. The virtual strain components are obtained by differentiation of the virtual displacement field using the following relationships in a given polar coordinate system

$$\varepsilon_r = \frac{\partial u_r}{\partial r}, \quad \varepsilon_\theta = \frac{1}{r}\frac{\partial u_\theta}{\partial \theta} + \frac{u_r}{r}, \quad \varepsilon_s = \frac{\partial u_\theta}{\partial r} + \frac{1}{r}\frac{\partial u_r}{\partial \theta} - \frac{u_\theta}{r} \tag{10}$$

In the present case, the virtual strain components are

$$\varepsilon_r^* = \varepsilon_\theta^* = -k, \quad \varepsilon_s^* = 0 \tag{11}$$

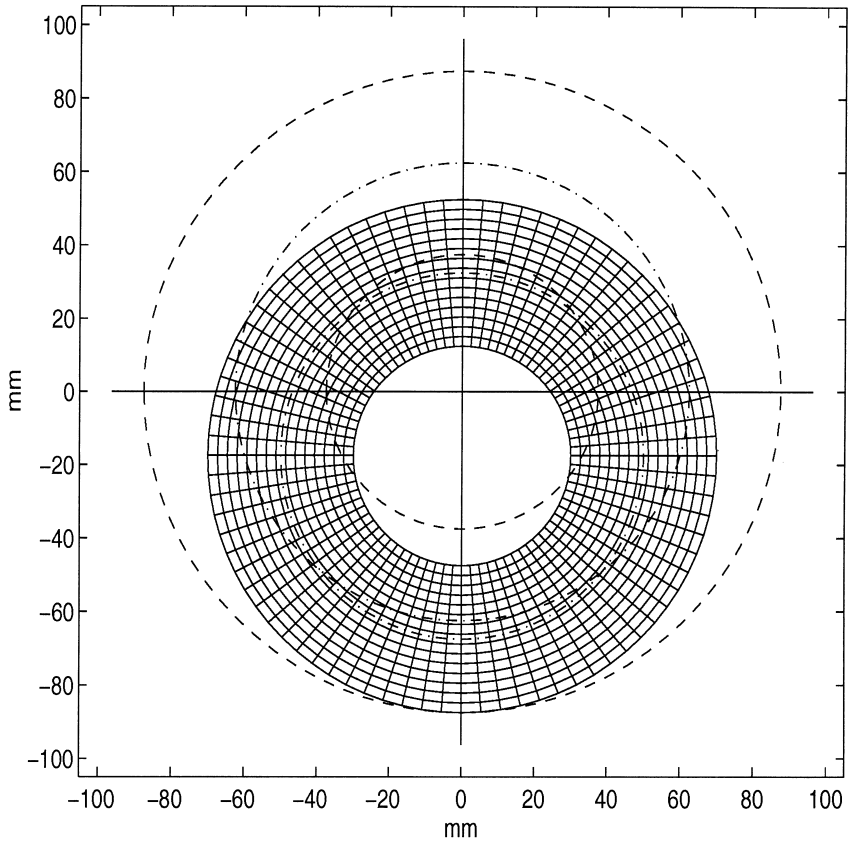

Fig. 6. Virtual hydrostatical compression of the ring specimen. Dashed line: undeformed specimen. $R_1 = 87.5$ mm, $R_0 = 37.5$ mm, $k = 0.2$.

The virtual displacement of point M is

$$\vec{u}^*(M) = -2kR_1\vec{e}_y \tag{12}$$

Finally, Eq. (4) becomes

$$Q_{\theta\theta}\int_0^{2\pi}\int_{R_0}^{R_1}\varepsilon_\theta r \,\mathrm{d}r\,\mathrm{d}\theta + Q_{rr}\int_0^{2\pi}\int_{R_0}^{R_1}\varepsilon_r r \,\mathrm{d}r\,\mathrm{d}\theta + Q_{\theta r}\int_0^{2\pi}\int_{R_0}^{R_1}(\varepsilon_r+\varepsilon_\theta) r \,\mathrm{d}r\,\mathrm{d}\theta = -\frac{2FR_1}{e} \tag{13}$$

As may be seen, only three among the four unknown stiffnesses are involved: Q_{rr}, $Q_{\theta\theta}$ and $Q_{\theta r}$.

2.4.2.2. Field 2: virtual bending. The second field describes a virtual bending of the circle (see Fig. 7). It is built under the Euler–Bernoulli's assumption to eliminate the contribution of Q_{rr} and Q_{ss}. Virtual displacements can be expressed as follows in the natural polar coordinate system

$$u_r^* = kR\,\cos\,2\theta, \quad u_\theta^* = 2k(r-R)\sin\,2\theta, \quad K = -kR \tag{14}$$

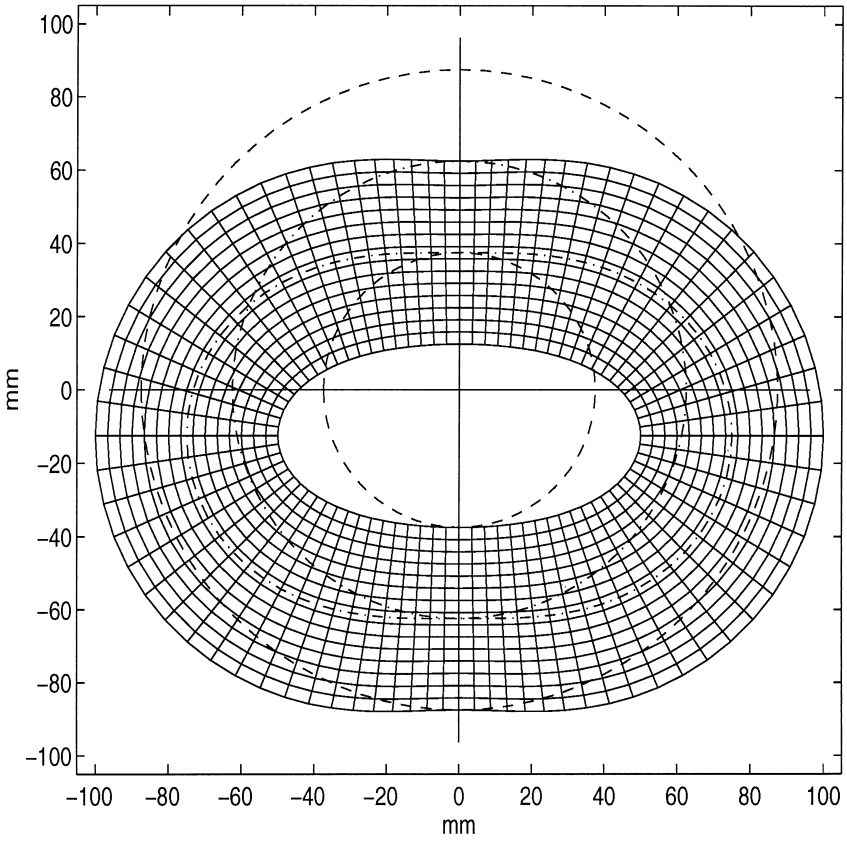

Fig. 7. Virtual bending of the ring specimen. Dashed line: undeformed specimen. $R_1 = 87.5$ mm, $R_0 = 37.5$ mm, $k = 0.2$.

The only non-zero virtual strain component corresponding to the above virtual displacement field is

$$\varepsilon_\theta^* = \frac{4k}{r}\left(r - \frac{3}{4}R\right)\cos\ 2\theta \tag{15}$$

The corresponding virtual displacement of point M is

$$\vec{u}^*(M) = -2kR\vec{e}_y \tag{16}$$

In this case, Eq. (5) becomes

$$Q_{\theta\theta}\int_0^{2\pi}\int_{R_0}^{R_1}\varepsilon_\theta\left(r - \frac{3}{4}R\right)\cos\ 2\theta\ \mathrm{d}r\ \mathrm{d}\theta + Q_{\theta r}\int_0^{2\pi}\int_{R_0}^{R_1}\varepsilon_r\left(r - \frac{3}{4}R\right)\cos\ 2\theta\ \mathrm{d}r\ \mathrm{d}\theta = F\frac{R}{2e} \tag{17}$$

Only two stiffnesses are involved here: $Q_{\theta\theta}$ and $Q_{\theta r}$.

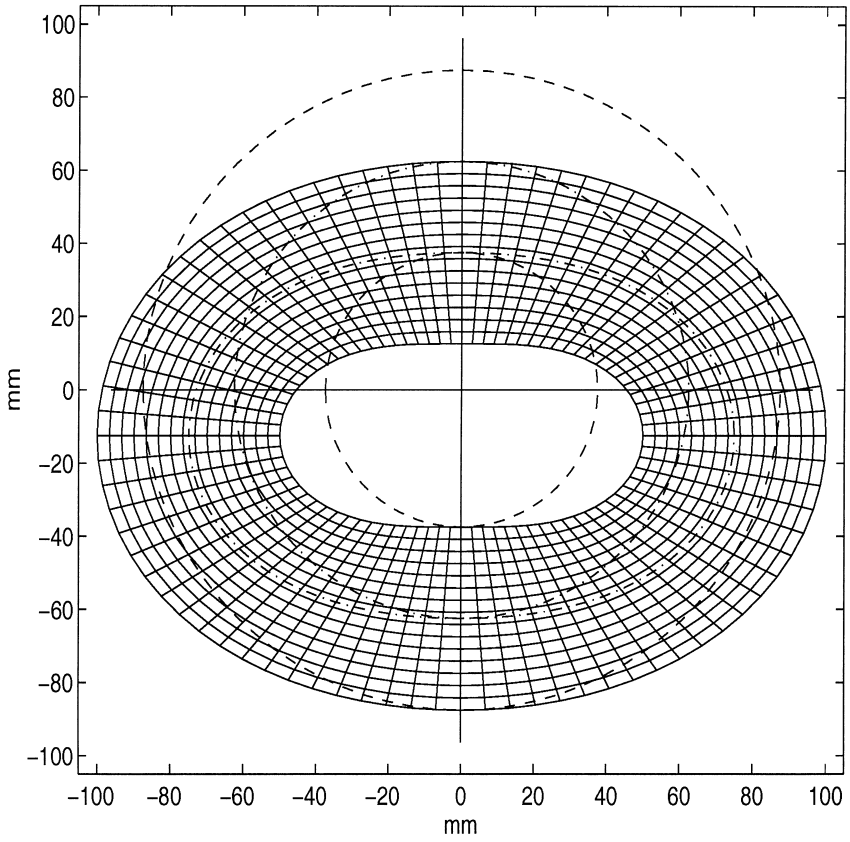

Fig. 8. Virtual shear of the ring specimen. Dashed line: undeformed specimen. $R_1 = 87.5$ mm, $R_0 = 37.5$ mm, $k = 0.2$.

2.4.2.3. Field 3: virtual shear. The third field (see Fig. 8) is such that only the shear strain is non-zero, so that only the shear modulus is involved in the internal virtual work. In the natural coordinate system, the virtual displacement field is

$$u_r^* = kR \cos 2\theta, \quad u_\theta^* = -\frac{k}{2}R \sin 2\theta, \quad K = -kR \tag{18}$$

The corresponding virtual shear strain field is

$$\varepsilon_s^* = -k\frac{3R}{2r} \sin 2\theta \tag{19}$$

The virtual displacement of point M is

$$\vec{u}^*(M) = -2kR\vec{e}_y \tag{20}$$

Eq. (5) reduces to

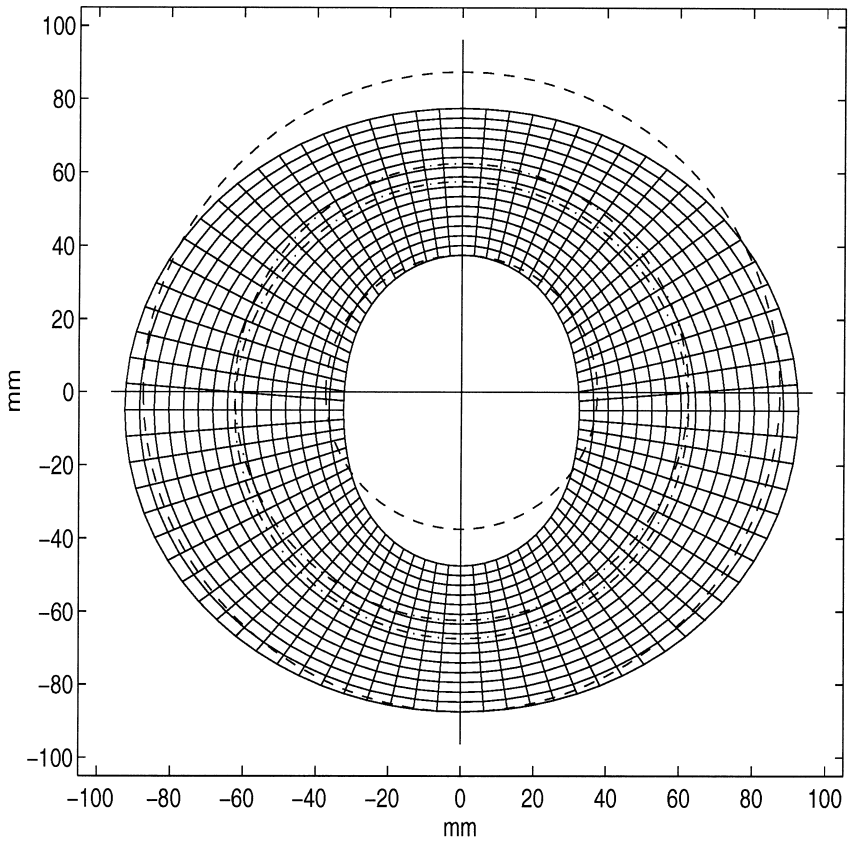

Fig. 9. Virtual swelling of the ring specimen. Dashed line: undeformed specimen. $R_1 = 87.5$ mm, $R_0 = 37.5$ mm, $k = 0.2$.

$$Q_{ss}\int_0^{2\pi}\int_{R_0}^{R_1}\varepsilon_s \ \sin\ 2\theta \ \mathrm{d}r \ \mathrm{d}\theta = -\frac{4}{3e}F \tag{21}$$

This equation is completely uncoupled, as only the shear stiffness is involved.

2.4.2.4. Field 4: virtual swelling. The fourth field describes a swelling of the circle (see Fig. 9). In the natural polar coordinate system, the virtual displacement field is

$$u_r^* = k(r - R)\cos\ 2\theta, \quad u_\theta^* = 0, \quad K = -\frac{kh}{2} \tag{22}$$

It leads to three non-zero virtual strain components

$$\varepsilon_r^* = k\ \cos\ 2\theta, \quad \varepsilon_\theta^* = k\left(1 - \frac{R}{r}\right)\cos\ 2\theta, \quad \varepsilon_s^* = -2k\left(1 - \frac{R}{r}\right)\sin\ 2\theta \tag{23}$$

The virtual displacement of point M is the same as in the previous cases

$$\vec{u}^*(M) = -kh\vec{e}_y \tag{24}$$

As a result, the four unknowns are related to the load applied to the circle

$$Q_{\theta\theta}\int_0^{2\pi}\int_{R_0}^{R_1}\varepsilon_\theta(r-R)\cos\ 2\theta\ \mathrm{d}r\ \mathrm{d}\theta + Q_{rr}\int_0^{2\pi}\int_{R_0}^{R_1}\varepsilon_r r\ \cos\ 2\theta\ \mathrm{d}r\ \mathrm{d}\theta + Q_{\theta r}\left[\int_0^{2\pi}\int_{R_0}^{R_1}\varepsilon_r(r-R)\cos\ 2\theta\ \mathrm{d}r\ \mathrm{d}\theta + \int_0^{2\pi}\int_{R_0}^{R_1}\varepsilon_\theta r\ \cos\ 2\theta\ \mathrm{d}r\ \mathrm{d}\theta\right] - 2Q_{ss}\int_0^{2\pi}\int_{R_0}^{R_1}\varepsilon_s(r-R)\sin\ 2\theta\ \mathrm{d}r\ \mathrm{d}\theta = F\frac{h}{e} \tag{25}$$

2.4.2.5. Conclusion. It has been shown that the application of the principle of virtual work with four independent virtual fields leads to a system of four partially uncoupled linear equations where the stiffnesses are unknown. This system can be written as follows

$$\mathbf{Aq} = \mathbf{b} \tag{26}$$

where **q** is the unknown vector

$$\mathbf{q}\text{:}\quad \{Q_{\theta\theta}, Q_{rr}, Q_{\theta r}, Q_{ss}\}^{\mathrm{T}} \tag{27}$$

A is the 4×4 matrix of the linear system:

$$\mathbf{A}\text{:}\quad \begin{pmatrix} A_{11} & A_{12} & A_{13} & 0 \\ A_{21} & 0 & A_{23} & 0 \\ 0 & 0 & 0 & A_{34} \\ A_{41} & A_{42} & A_{43} & A_{44} \end{pmatrix} \tag{28}$$

with

$$A_{11} = \int_0^{2\pi}\int_{R_0}^{R_1}\varepsilon_\theta r\ \mathrm{d}r\ \mathrm{d}\theta, \quad A_{12}\int_0^{2\pi}\int_{R_0}^{R_1}\varepsilon_r r\ \mathrm{d}r\ \mathrm{d}\theta, \quad A_{13} = \int_0^{2\pi}\int_{R_0}^{R_1}(\varepsilon_r+\varepsilon_\theta) r\ \mathrm{d}r\ \mathrm{d}\theta$$

$$A_{21} = \int_0^{2\pi}\int_{R_0}^{R_1}\varepsilon_\theta\left(r-\frac{3}{4}R\right)\cos\ 2\theta\ \mathrm{d}r\ \mathrm{d}\theta, \quad A_{23} = \int_0^{2\pi}\int_{R_0}^{R_1}\varepsilon_r\left(r-\frac{3}{4}R\right)\cos\ 2\theta\ \mathrm{d}r\ \mathrm{d}\theta$$

$$A_{34} = \int_0^{2\pi}\int_{R_0}^{R_1}\varepsilon_s\ \sin\ 2\theta\ \mathrm{d}r\ \mathrm{d}\theta$$

$$A_{41} = \int_0^{2\pi}\int_{R_0}^{R_1}\varepsilon_\theta(r-R)\cos\ 2\theta\ \mathrm{d}r\ \mathrm{d}\theta, \quad A_{42} = \int_0^{2\pi}\int_{R_0}^{R_1}\varepsilon_r r\ \cos\ 2\theta\ \mathrm{d}r\ \mathrm{d}\theta$$

$$A_{43} = \int_0^{2\pi}\int_{R_0}^{R_1}[\varepsilon_r(r-R)+\varepsilon_\theta r]\cos\ 2\theta\ \mathrm{d}r\ \mathrm{d}\theta, \quad A_{44} = -2\int_0^{2\pi}\int_{R_0}^{R_1}\varepsilon_s(r-R)\sin\ 2\theta r\ \mathrm{d}r\ \mathrm{d}\theta \tag{29}$$

and **b** is the right-hand-side vector:

$$\mathbf{b}: \quad F \times \left\{ -\frac{2R_1}{e}, \frac{R}{2e}, -\frac{4}{3e}, \frac{h}{e} \right\}^{\mathrm{T}} \tag{30}$$

As may be seen, two equations are partially uncoupled and one is completely uncoupled. This result illustrates the above rule (3).

2.4.3. Conclusion

A system of four linear equations has been built up. The purpose of the next section is to validate the present approach using some finite element simulations. Strain fields provided by the finite element model of the specimen are considered as input data to compute the integrals in matrix **A**. Stiffness components are finally back-identified and compared to the input values of the finite element model to assess the accuracy and the stability of the procedure.

3. Numerical simulations

3.1. Identification

The output data of the finite element calculation described in Section 2.3 in terms of strains at the centroid of each element are considered as input data for the identification programme.

The integrals of the strain components in matrix **A** are transformed into sums. For instance, the following integral becomes

$$\int_0^{2\pi}\int_{R_0}^{R_1} \varepsilon_r (r-R)\cos 2\theta \, \mathrm{d}r \, \mathrm{d}\theta = \left(\sum_{\mathrm{m}=1}^{\mathrm{N}_\theta}\sum_{\mathrm{n}=1}^{\mathrm{N}_\mathrm{r}} \varepsilon_r^{\mathrm{mn}} (r^{\mathrm{mn}} - R)\cos 2\theta^{\mathrm{mn}} \right) \Delta r \Delta\theta$$

$$= \sum_{\mathrm{m}=1}^{\mathrm{N}_\theta}\sum_{\mathrm{n}=1}^{\mathrm{N}_\mathrm{r}} (\Theta_1^{\mathrm{mn}} \varepsilon_r^{\mathrm{mn}} R_2^{\mathrm{mn}}) \frac{2h\pi}{N_r N_\theta} \tag{31}$$

where N_r, N_θ are the number of elements along the width and the circle, respectively. Applying this approximation to the remaining integrals, matrix **A** can be written as follows

$$\begin{pmatrix} \displaystyle\sum_{\mathrm{m}=1}^{\mathrm{N}_\theta}\sum_{\mathrm{n}=1}^{\mathrm{N}_\mathrm{r}} \varepsilon_\theta^{\mathrm{mn}} r^{\mathrm{mn}} & \displaystyle\sum_{\mathrm{m}=1}^{\mathrm{N}_\theta}\sum_{\mathrm{n}=1}^{\mathrm{N}_\mathrm{r}} \varepsilon_r^{\mathrm{mn}} r^{\mathrm{mn}} & \displaystyle\sum_{\mathrm{m}=1}^{\mathrm{N}_\theta}\sum_{\mathrm{n}=1}^{\mathrm{N}_\mathrm{r}} (\varepsilon_r^{\mathrm{mn}} + \varepsilon_\theta^{\mathrm{mn}}) r^{\mathrm{mn}} & 0 \\ \displaystyle\sum_{\mathrm{m}=1}^{\mathrm{N}_\theta}\sum_{\mathrm{n}=1}^{\mathrm{N}_\mathrm{r}} \Theta_1^{\mathrm{mn}} \varepsilon_\theta^{\mathrm{mn}} R_1^{\mathrm{mn}} & 0 & \displaystyle\sum_{\mathrm{m}=1}^{\mathrm{N}_\theta}\sum_{\mathrm{n}=1}^{\mathrm{N}_\mathrm{r}} \Theta_1^{\mathrm{mn}} \varepsilon_r^{\mathrm{mn}} R_1^{\mathrm{mn}} & 0 \\ 0 & 0 & 0 & \displaystyle\sum_{\mathrm{m}=1}^{\mathrm{N}_\theta}\sum_{\mathrm{n}=1}^{\mathrm{N}_\mathrm{r}} \Theta_2^{\mathrm{mn}} \varepsilon_s^{\mathrm{mn}} \\ \displaystyle\sum_{\mathrm{m}=1}^{\mathrm{N}_\theta}\sum_{\mathrm{n}=1}^{\mathrm{N}_\mathrm{r}} \Theta_1^{\mathrm{mn}} \varepsilon_\theta^{\mathrm{mn}} R_2^{\mathrm{mn}} & \displaystyle\sum_{\mathrm{m}=1}^{\mathrm{N}_\theta}\sum_{\mathrm{n}=1}^{\mathrm{N}_\mathrm{r}} \Theta_1^{\mathrm{mn}} \varepsilon_r^{\mathrm{mn}} r^{\mathrm{mn}} & \displaystyle\sum_{\mathrm{m}=1}^{\mathrm{N}_\theta}\sum_{\mathrm{n}=1}^{\mathrm{N}_\mathrm{r}} \Theta_1^{\mathrm{mn}} (\varepsilon_r^{\mathrm{mn}} R_2^{\mathrm{mn}} + \varepsilon_\theta^{\mathrm{mn}} r^{\mathrm{mn}}) & -2\displaystyle\sum_{\mathrm{m}=1}^{\mathrm{N}_\theta}\sum_{\mathrm{n}=1}^{\mathrm{N}_\mathrm{r}} \Theta_2^{\mathrm{mn}} \varepsilon_s^{\mathrm{mn}} R_2^{\mathrm{mn}} \end{pmatrix} \tag{32}$$

with

Table 1
Actual and identified values of the stiffness components

	$E_{\theta\theta}$ GPa	E_{rr} GPa	$G_{\theta r}$ GPa	$\nu_{\theta r}$
Actual value	40.00	10.00	4.00	0.30
Identified value	40.16	9.97	4.00	0.297
Relative difference %	0.4	−0.3	0.0	−1.0

$$\Theta_1^{mn} = \cos\ 2\theta^{mn}, \quad \Theta_2^{mn} = \sin\ 2\theta^{mn} \tag{33}$$

$$R_1^{mn} = r^{mn} - \tfrac{3}{4}R, \quad R_2^{mn} = r^{mn} - R \tag{34}$$

and ε_r^{mn}, ε_θ^{mn}, ε_s^{mn} are the same values of the three strain components over each element.

The right-hand-side vector is finally written as

$$\mathbf{b}: \quad F\frac{N_r N_\theta}{2\pi e h}\left\{-2R_1, \frac{1}{2}R, -\frac{4}{3}, h\right\}^{T} \tag{35}$$

The linear system is solved in order to identify the stiffness components $Q_{\theta\theta}$, Q_{rr}, $Q_{\theta r}$ and Q_{ss}. $E_{\theta\theta}$, E_{rr}, $G_{\theta r}$ and $\nu_{\theta r}$ are the obtained with Eq. (6). The magnitude of the applied loading F is 200,000 N. The results are reported in Table 1. As can be seen, the identified values agree within less than 1% to the reference values. This result validates the procedure from a theoretical point of view.

3.2. Stability

As the present identification method will be used in experimental applications, it is important to check its stability as the strain components cannot be exactly collected in practice. Therefore, experimental errors have been numerically simulated by adding noise to the strain components. This noise is modelled with a truncated normal distribution of errors supposed to simulate experimental errors. Two magnitudes have been chosen, 5 and 10% of the maximum strain component for each of three strain components. The standard deviation of the error distribution is also computed. These perturbated data considered as input data for the identification programme and the corresponding identified stiffnesses are collected. The process is repeated 50 times to obtain a distribution of perturbated identified stiffnesses. To check the stability, the amplitude and mean of these identified distributions have been compared to the original input stiffnesses and to the perturbation amplitude. The calculations have been performed for both amplitudes of errors. The coefficient of variation, which is defined by the ratio between the standard deviation and the mean, is also computed in each case. This quantity is directly related to the scatter of the distribution. The results are reported in Tables 2 and 3. It can be seen that

Table 2
Identified stiffnesses distributions from 5% perturbated strains

	$E_{\theta\theta}$ GPa	E_{rr} GPa	$G_{\theta r}$ GPa	$\nu_{\theta r}$
Actual values	40.00	10.00	4.00	0.30
Perturbated values	40.36	9.88	4.00	0.29
Difference (%)	0.9	−1.2	0.0	−2.7
Coefficient of variation (%)	4.8	5.2	0.3	20.3

Table 3
Identified stiffness distributions from 10% perturbated strain components

	$E_{\theta\theta}$ GPa	E_{rr} GPa	$G_{\theta r}$ GPa	$\nu_{\theta r}$
Reference values	40.00	10.00	4.00	0.30
Perturbated values	40.37	9.82	4.00	0.27
Difference (%)	0.9	−1.7	−0.0	−10.0
Coefficient of variation (%)	12.0	13.1	0.8	60.8

the difference between the mean value of the identified moduli computed from the perturbated strain components and the actual corresponding quantities is lower than 1.7%. Poisson's ratio is obtained with a relative difference of 10% in the second case. This last result is in agreement with the conclusions of previous studies carried out on other specimen shapes and loading conditions, in which it was shown that the lowest accuracy is obtained with Poisson's ratio because of its small influence on the strain and stress fields. It must be emphasized that the coefficients of variation remain reasonably low for $Q_{\theta\theta}$, Q_{rr}, and Q_{ss} even for the 10% perturbation. This is due to the fact that the integrals can be interpreted as weighted means of the strain components that average out local variations.

4. Conclusion

An identification method has been proposed for determining the through-thickness stiffnesses of thick laminated composites. These properties are difficult to measure with standard methods and such alternative approaches can, therefore, be considered advantageously.

The main features of the present method are:

- heterogeneous stress and strain fields are considered and processed;
- no assumption is made concerning the displacement field;
- the whole strain field is considered as input data of the identification procedure;
- only one test is required to determine the four independent parameters;
- the method itself is based on a relevant use of the principle of virtual work with four independent fields;
- the method is direct and neither finite element model nor iterative calculations are required;
- the accuracy and the stability of the procedure have been studied and the results can be considered compatible with a practical application.

One could think that the main difficulty lies in the whole strain field measurement that is performed in practice with a suitable optical method. However, such setups now become more popular, reliable and inexpensive. Previous similar studies on other specimen shapes and loading conditions for measuring in-plane and bending stiffnesses of thin composite have been successfully carried out with deflectometry setups or grid techniques (Grédiac, 1998b, 1999). As a result, one can expect to actually measure the through-thickness moduli of thick rings with the present approach.

References

Araujo, A.L., Mota Soares, C.M., Freitas, M.J.M., 1996. Characterization of material parameters of composite specimens using optimization and experimental data. Composites Part B 27B (2), 185–191.

ASTM, 1998. Standard test method for measuring the curved beam strength of a fiber-reinforced polymer–matrix composite (draft number 5). ASTM D5379-93.

Broughton, W.R., Sims, G.D., 1994. An overview of through-thickness test methods for polymer matrix composites. NPL Report DMMA(A) 148, National Laboratory, UK.

Cunha, J., Piranda, J., 1999. Application of model updating techniques in dynamics for the identification of elastic constants of composite materials. Composites Part B 30B, 79–85.

De Wilde, W.P., 1991. Identification of the rigidities of composite systems by mixed numerical/experimental methods. In: Mechanical Identification of Composites. Elsevier, Amsterdam, pp. 1–15.

Frederiksen, P.S., 1997. Numerical studies for identification of orthotropic elastic constants of thick plates. European Journal of Mechanics A/Solids 16, 117–140.

Frederiksen, P.S., 1998. Parameters uncertainty for estimation of elastic constants. International Journal of Solids and Structures 35, 1241–1260.

Gipple, K.L., Hoyns, D., 1994. Measurement of the out-of-plane shear response of thick section composite materials using the V-notched beam specimen. Journal of Composite Materials 28 (6), 543–572.

Grédiac, M., 1989. Principe des travaux virtuels et identification/Principle of virtual work and identification. Comptes rendus de l'Académie des Sciences. II/309, pp. 1–5. In French with abridged English version.

Grédiac, M., 1996. On the direct determination of invariant parameters governing the bending of anisotropic plates. International Journal of Solids and Structures 33 (27), 3969–3982.

Grédiac, M., Pierron, F., 1998. A T-shaped specimen for the direct characterization of orthotropic materials. International Journal for Numerical Methods in Engineering 41, 293–309.

Grédiac, M., Fournier, N., Paris, P-A., Surrel, Y., 1998a. Direct identification of elastic constants of anisotropic plates by modal analysis: experiments and results. Journal of Sound and Vibration 210 (5), 645–659.

Grédiac, M., Fournier, N., Paris, P-A., Surrel, Y., 1998b. Direct measurement of invariant parameters of composite plates. *Journal of Composite Materials*. in press.

Grédiac, M., Pierron, F., Surrel, Y., 1999. Novel procedure for complete in-plane composite characterization using a T-shaped specimen. *Experimental Mechanics* 39, 142–149.

Hendriks, M.A.N., 1991. Identification of the mechanical properties of solid materials. Ph.D. thesis, Eindhoven University of Technology.

Hiel, C., Surnish, M., Chappell, D., 1991. A curved beam specimen for determining the interlaminar tensile strength of a laminated composite. Journal of Composite Materials 25, 854–868.

Mespoulet, S., 1998. Through-thickness test methods for laminated composite materials. Ph.D. thesis, Imperial College of Science, Technology and Medicine.

Pedersen, P., Frederiksen, P.S., 1992. Identification of orthotropic materials moduli by combinated experimental numerical approach. Measurements 10, 113–118.

Pierron, F., Davies, P., 1998. Ring compression test for cylindrical composite mechanical characterization. *Proceedings of the CTS4 Conference* (Composite Testing and Standardization), 31 August–2 September 1998 in Lisbon, Portugal, pp. 193–202.

Rikards, R., Chate, A., 1998. Identification of elastic properties of composites by method of planning of experiments. Composite Structures 42 (3), 257–263.

Sol, H., 1986. Identification of anisotropic plates rigidities using free vibration data. Ph.D. thesis, Free University of Brussels.